Inorganic Chemistry
Article

Inorg. Chem. **2010**, *49*, 1705–1711 **1705**
DOI: 10.1021/ic902128g

A Bioinspired Approach to the Synthesis of Bimetallic CoNi Nanoparticles

Natividad Gálvez,*,† Elsa Valero,† Marcelo Ceolin,‡ Susana Trasobares,§ Miguel López-Haro,§ José J. Calvino,§ and José M. Domínguez-Vera†

†*Departamento de Química Inorgánica, Facultad de Ciencias, Universidad de Granada, 18071 Granada, Spain,* ‡*Instituto de Físico-Química Teórica y Aplicada, Universidad Nacional de La Plata, Argentina, and* §*Departamento Ciencia de Materiales e Ingeniería Metalúrgica y Química Inorgánica, Universidad de Cádiz, Campus Río San Pedro, 11510 Cádiz, Spain*

Received October 27, 2009

Bimetallic CoNi nanoparticles have been prepared within the apoferritin cavity. The protein shell controls size, prevents aggregation, and makes nanoparticles water-soluble. The CoNi series prepared in this way were structurally and magnetically characterized, the resulting magnetic properties varying accordingly with composition (Co_{75}/Ni_{25}, Co_{50}/Ni_{50}, Co_{25}/Ni_{75}). Co and Ni metals were associated in each nanoparticle, as demonstrated by high-angle annular dark field scanning electron microscopy and electron energy loss spectroscopy (EELS). After intentional oxidation, the CoNi nanoparticles were characterized by EELS, X-ray absorption near edge structure (XANES), and SQUID measurements to evaluate the importance of the oxidation on magnetic properties.

Introduction

Metallic nanoparticles remain the focus of numerous studies because of their size-dependent electronic, optical, catalytic, and magnetic properties. Specifically, magnetic properties can be used in a variety of applications ranging from magnetic data storage to probes and vectors for biomedical sciences.[1]

The ability to manufacture and control the structure and composition of metallic nanoparticles will allow the design of materials with desirable properties. In particular, alloy-based magnetic nanoparticles constitute an extremely appealing class of materials, since their magnetic properties can be tuned by combining size effects and alloy composition.[2] The challenge of being able to fabricate materials with well-defined, controllable properties on the nanometer scale has generated interest in the preparation of bimetallic and trimetallic nanoparticles.[2,3] The synthesis of bimetallic nanoparticles or clusters is far from easy, because of the difficulty of controlling both particle stoichiometry and surface state.[4] Bimetallic ferromagnetic CoNi nanoparticles are of particular interest for their potential to overcome the superparamagnetic limit for ultra-high-density magnetic recording and to enhance contrast in magnetic resonance imaging.[2] To our knowledge, apart from a sonochemical method reported by Gedanken et al. in 1998,[5] only four main examples can be found in the literature exploring chemical routes for the synthesis of CoNi nanoparticles with varying compositions: (1) a sol−gel route for the preparation of CoNi nanoclusters hosted in silica gel,[6] (2) an alginate-mediated growth of CoNi nanoparticles,[7] (3) a cobalt−nickel reduction in liquid polyol,[8] and (4) a "guest−host" strategy using layered double hydroxides as a host.[9]

Because magnetic properties are strongly size- and shape-dependent in the nanometer regime, methods that yield nanoparticles of uniform size and shape are extremely important. One possible route for obtaining nonaggregated size- and shape-controlled metallic nanoparticles is the use of a preorganized molecular matrix as a chemical and spatial nanocage for their construction. Typical examples of this type of molecule are apoferritin and small ferritin cages.[10]

*To whom correspondence should be addressed. E-mail: ngalvez@ugr.es.

(1) (a) Jun, Y.; Choi, J.; Cheon, J. *Chem. Commum*. **2007**, 1203. (b) Jun, Y.; Seo, J.; Cheon, J. *Acc. Chem. Res*. **2008**, *41*, 179.
(2) Fernando, R.; Jellinek, J.; Johnston, R. L. *Chem. Rev*. **2008**, *108*, 845 and references therein.
(3) Wen, M.; Liu, Q.; Wang, Y.; Zhu, Y.; Wu, Q. *Colloids Surf., A* **2008**, *318*, 238.
(4) Zitoun, D.; Respaud, M.; Fromen, M. C.; Casanove, M. J.; Lecante, P.; Amiens, C.; Chaudret, B. *Phys. Rev. Lett*. **2002**, *89*, 037203.
(5) Shafi, K.V. P.; Gedanken, A.; Prozorov, R. *J. Mater. Chem*. **1998**, *8*, 769.
(6) Mattei, G.; de Julián Fernández, C.; Mazzoldi, P.; Sada, C.; De, G.; Battaglin, G.; Sangregorio, C.; Gatteschi, D. *Chem. Mater*. **2002**, *14*, 3440.
(7) Brayner, R.; Vaulay, M.-J.; Fiévet, F.; Coradin, T. *Chem. Mater*. **2007**, *19*, 1190.
(8) Ung, D.; Soumare, Y.; Chakroune, N.; Viau, G.; Vaulay, M.-J.; Richard, V.; Fiévet, F. *Chem. Mater*. **2007**, *19*, 2084.
(9) Tarasov, K. A.; Isupov, V. P.; Bokhonov, B. B.; Gaponov, Y. A.; Tolochko, B. P.; Yulikov, M. M.; Yudanov, V. F.; Davidson, A.; Beaunier, P.; Marceau, E.; Che, M. *Microporous Mesoporous Mater*. **2008**, *107*, 202.
(10) (a) Mann, S. *Biomimetic Materials Chemistry*; Wiley: New York, 1996. (b) Douglas, T.; Strable, E.; Willits, D.; Aitouchen, A.; Libera, M.; Young, M. *Adv. Mater*. **2002**, *14*, 415. (c) Douglas, T.; Stark, V. T. *Inorg. Chem*. **2000**, *39*, 1828. (d) Wong, K. K. W.; Douglas, T.; Gider, S.; Awschalom, D. D.; Mann, S. *Chem. Mater*. **1998**, *10*, 279.

Published on Web 01/12/2010

Apoferritin consists of a spherical protein shell composed of 24 subunits surrounding an aqueous cavity with a diameter of about 8 nm.[11] The high stoichiometry binding of some metal ions to the inner cavity wall of apoferritin[12] and the capacity of these bonded metal ions to be reduced by the appropriate chemical reagent give rise to the nucleation of zero-valent metallic nanoparticles.[13] In this way, several metallic nanoparticles have been prepared using ferritin protein as a template biomolecule.[14]

Our group has previously reported the use of the apoferritin cavity to prepare magnetic Co, Ni, and Pd nanoparticles as well as Cu and Ag nanoparticles with optical properties.[15]

We report here a simple bioinspired procedure, using the apoferritin protein, for the synthesis of monodisperse Co_xNi_y nanoparticles of variable composition. Detailed compositional and magnetic characterization of these bimetallic CoNi nanoparticles is presented.

Experimental Section

Bimetallic nanoparticles with theoretical final atomic ratios of 75:25, 50:50, and 25:75 Co/Ni were prepared by adding 1 mL of a 0.1 M solution of mixed $CoSO_4/NiSO_4$ salts to a 4 mg/mL apoferritin (horse spleen apoferritin, 49 mg/mL, Sigma Aldrich) solution and incubating the sample for 24 h. The resulting solutions were clear and homogeneous. The pH was dynamically adjusted to 8 with 0.1 M NaOH to increase the amount of M^{2+} per protein cage, thanks to the well-known fact of the existence of an out−in negative charge gradient from the external shell to the cavity.[16] All solutions were carefully degassed previous to incubation.

The solutions were passed through a calibrated G-25 Sephadex column (1.5 cm × 5.5 cm; Scheme 1). The apoferritin-containing fractions were isolated ($Co^{2+}Ni^{2+}$−apoferritin), and metals and protein contents were then determined by atomic absorption spectroscopy and by absorbance at 280 nm (ε = 468 000 $cm^{-1}M^{-1}$), respectively. The addition of $NaBH_4$ (0.1 mL, 4 mg/mL) to the mixture of $Co^{2+}Ni^{2+}$−apoferritin produced black solutions of Co^0Ni^0−apoferritin. The solutions were dialyzed against milli-Q water and finally lyophilized to yield black powders of CoNi nanoparticles.

Samples used for transmission electron microscopy (TEM) study were prepared by placing a drop onto a carbon-coated Cu grid and drying it in a glovebox. Electron micrographs were taken with a Philips CM-20 HR analytical electron microscope operating at 200 keV. High-angle annular dark field scanning electron microscopy (HAADF-STEM) and electron energy-loss spectra (EELS) were recorded on a JEOL2010F working at 200 K eV. The spectrum line (SL) mode, which consists of acquiring a series of EELS spectra while a 0.5 nm beam with a current of 0.1−0.3 nA is scanned along the sample, was used. The HAADF signal was also simultaneously collected at each point within the scanned area. This approach allows correlating nanoanalytical and structural information of the region under study.

X-ray absorption spectroscopy experiments were performed at the D04B-XAFS1 experimental stations of the Synchrotron Light National Laboratory (LNLS), Campinas, Brazil. Nickel and cobalt K-edge experiments were performed at room temperature (ca. 22 °C) in transmission geometry using metal foils for calibration purposes. Data reduction and model fitting were performed using the program ATHENA from the IFFEFIT package.[17]

Magnetization measurements were performed on lyophilized samples using a magnetometer (Quantum Design MPMS-XL-5) equipped with a SQUID sensor. The temperature was varied between 2 and 300 K, according to a classical zero-field-cooled/field-cooled (ZFC/FC) procedure in the presence of a weak applied magnetic field (5 mT), and the hysteresis loops were obtained at 2 and 300 K in a magnetic field varying from +5 T to −5 T. Also, hysteresis loops after the field-cooling procedure (H = 5 T) were obtained at 2 K.

Scheme 1. Preparation of Apoferritin Encapsulated Bimetallic CoNi Nanoparticles

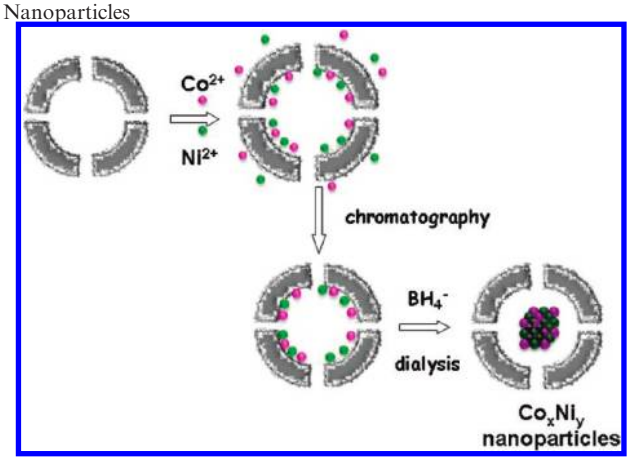

Table 1. Initial Co/Ni Molar Ratio Introduced during the Synthesis and Final Co/Ni Atomic Ratio Obtained by Atomic Absorption Spectroscopy

	initial Co/Ni	final Co/Ni
$Co_{25}Ni_{75}$	0.33	0.46
$Co_{50}Ni_{50}$	1	0.95
$Co_{75}Ni_{25}$	3	3.3
$*Co_{100}$		
$*Ni_{100}$	0	0

Results and Discussion

A series of bimetallic nanoparticles with different Co/Ni ratios (Co_{75}/Ni_{25}, Co_{50}/Ni_{50}, Co_{25}/Ni_{75}) were prepared using the apoferritin protein as a nanoreactor where growth is spatially limited by the protein cavity size. In this way, apoferritin was incubated with different Co/Ni proportions (75:25, 50:50 and 25:75) at pH 8 for 24 h. The protein-containing fractions were isolated by size exclusion chromatography and reduced by the addition of excess $NaBH_4$ (Scheme 1). The so-obtained black homogeneous solutions were dialyzed to eliminate unreacted products. The three CoNi metallic apoferritin samples were characterized by UV−vis spectroscopy, size exclusion chromatography (SEC), TEM, HAADF-STEM, EELS, X-ray absorption near edge structure (XANES), and SQUID techniques.

(11) (a) Harrison, P. M.; Arosio, P. *Biochim. Biophys. Acta* **1996**, *1275*, 161. (b) Proulx-Curry, P. M.; Chaspeen, N. D. *Coord. Chem. Rev.* **1995**, *144*, 347.
(12) Pead, S.; Durrant, E.; Webb, B.; Larsen, C.; Heaton, D.; Johnson, J.; Watt, G. D. *J. Inorg. Biochem.* **1995**, *59*, 15.
(13) Ueno, T.; Suzuki, M.; Goto, T.; Matsumoto, T.; Nagayama, K.; Watanabe, Y. *Angew. Chem., Int. Ed.* **2004**, *43*, 2527.
(14) Uchida, M.; Klem, M. T.; Allen, M.; Suci, P.; Flenniken, M.; Gillitzer, E.; Varpness, Z.; Liepold, L. O.; Young, M.; Douglas, T. *Adv. Mater.* **2007**, *19*, 1025 and references therein.
(15) (a) Gálvez, N.; Sánchez, P.; Domínguez-Vera, J. M. *Dalton Trans.* **2005**, 2492. (b) Clemente-León, M.; Coronado, E.; Soriano-Portillo, A.; Gálvez, N.; Domínguez-Vera, J. M. *J. Mater. Chem.* **2007**, *17*, 49. (c) Domínguez-Vera, J. M.; Gálvez, N.; Sánchez, P.; Mota, A. J.; Trasobares, S.; Hernández, J. C.; Calvino, J. J. *Eur. J. Inorg. Chem.* **2007**, 4823.
(16) Douglas, T.; Ripoll, D. R. *Protein Sci.* **1998**, *7*, 1083.
(17) Newville, M. *J. Synchrotron Radiat.* **2001**, *8*, 322.

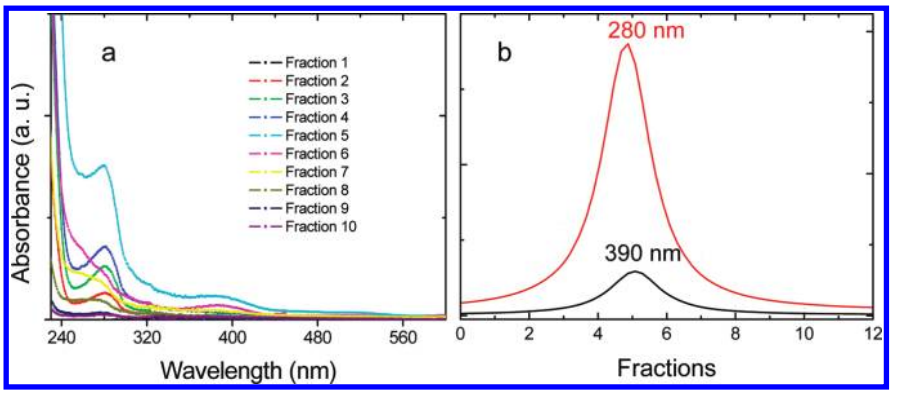

Figure 1. (a) UV−vis spectroscopy of the eluted fractions for the $Co_{75}Ni_{25}$ sample. (b) Size exclusion chromatography coelution profile for the same sample monitored at 280 (red) and 390 nm (black).

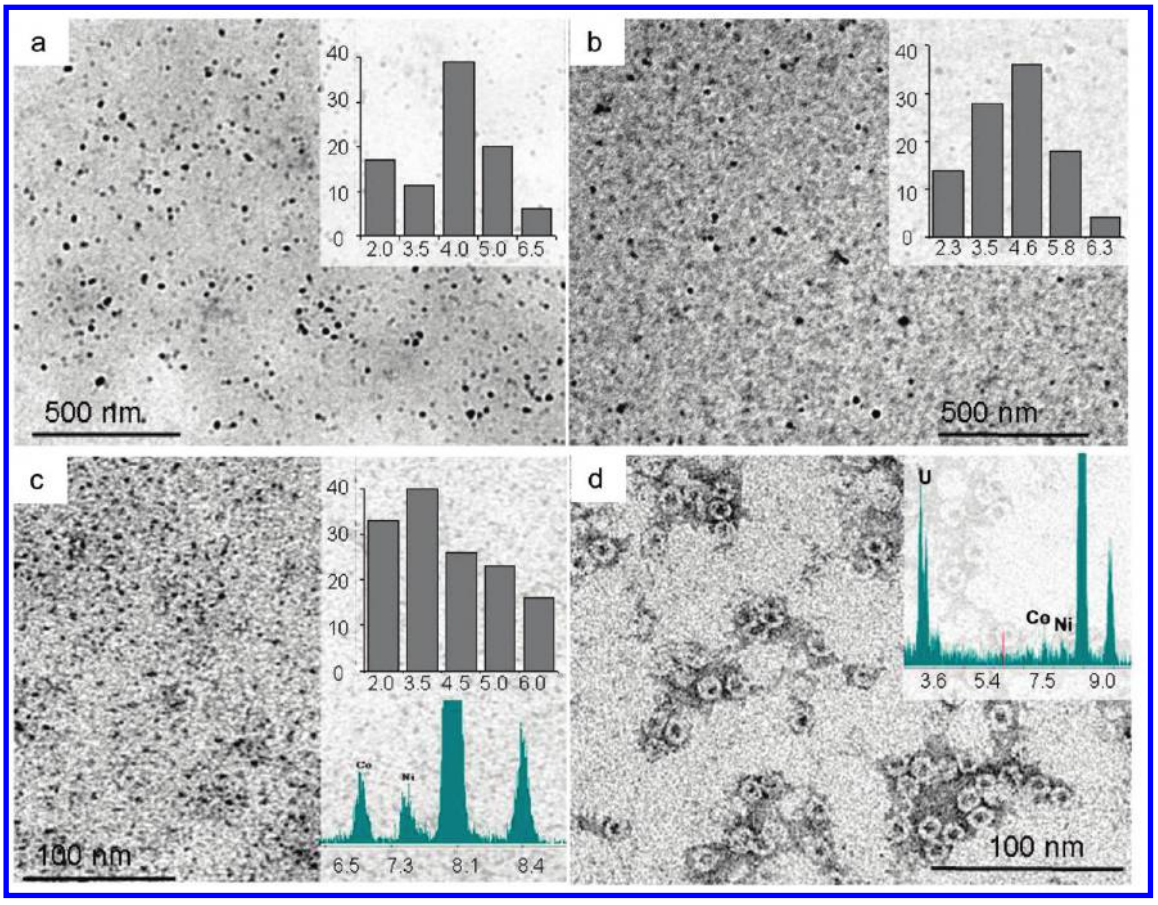

Figure 2. TEM micrographs of (a) $Co_{25}Ni_{75}$, (b) $Co_{50}Ni_{50}$, and (c) $Co_{75}Ni_{25}$ showing spherical nanoparticles and (d) $Co_{50}Ni_{50}$ stained with uranyl acetate. Inset: Particle size histograms and EDX spectra.

The eluted fractions obtained by SEC were analyzed by UV−vis spectroscopy. As an example, the evolution of the optical spectra of the $Co_{75}Ni_{25}$ sample is shown in Figure 1a. The band at 280 nm corresponds with the protein and the band at 390 nm with the metallic core. The spectrum of empty apoferritin did not show absorption at 390 nm. The band at 390 nm is a qualitative indication that metallic reduction took place. The coelution of protein and metal (Figure 1b) indicates that both the protein and metallic core are intimately associated after reduction.[18] The chemical composition of bimetallic nanoparticles was quantified by atomic absorption spectroscopy and by EDX spectroscopy. The final Co/Ni ratios in the nanoparticles are close to those present in the initial mixture (Table 1). Therefore, one can infer from these data that the final amount of encapsulated cations is directly related to the Co/Ni ratio introduced in the starting solution.

The TEM micrographs of the three samples $Co_{75}Ni_{25}$, $Co_{50}Ni_{50}$, and $Co_{25}Ni_{75}$ are shown in Figure 2. Measuring 50 nanoparticles from each sample showed no significant difference in particle size among the different samples. The metallic cores are generally spherical in shape. The mean diameter was statistically measured to be 4 ± 2.1, 4.5 ± 1.6,

(18) Klem, M. T.; Willits, D.; Solis, D. J.; Belcher, A. M.; Young, M.; Douglas, T. *Adv. Funct. Mater.* **2005**, *15*, 1489.

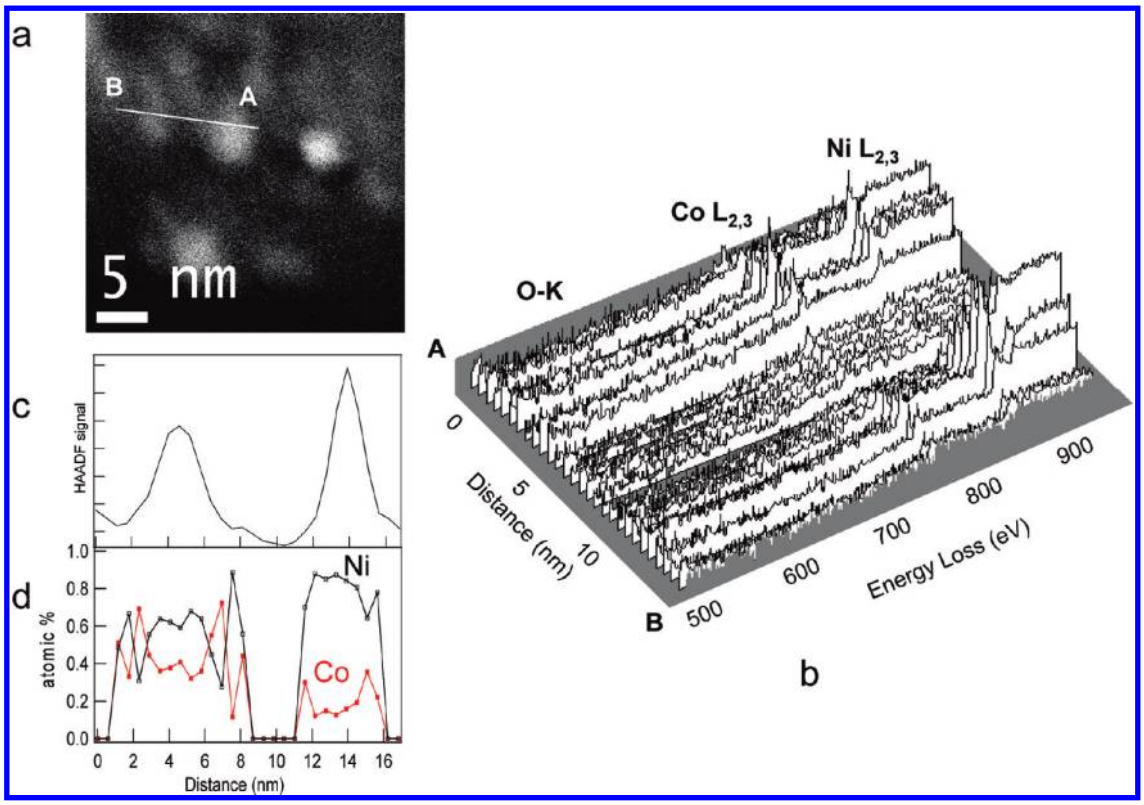

Figure 3. (a) STEM-HAADF image showing the two $Co_{25}Ni_{75}$ nanoparticles where the spectrum line analysis was performed. (b) 3D illustration of a set of 30 EEL spectra taken along the A−B line at the energy loss region of Co/$L_{2,3}$, Ni/$L_{2,3}$, and O/K edges (due to the small size of analyzed particles, we cannot rule out, completely, the presence of small amounts of the corresponding oxides). (c) HAADF signal intensity variation acquired simultaneously with the spectrum line shown in b. (d) Co and Ni chemical composition variation along both particles. In red line, the Co atomic ratio and, in black, the Ni atomic ratio.

and 3.9 ± 1.6 nm for $Co_{25}Ni_{75}$, $Co_{50}Ni_{50}$, and $Co_{75}Ni_{25}$, respectively. EDX confirmed the presence of Co and Ni (Figure 2c and d, inset), which were not detected outside the particles. When negatively stained with uranyl acetate, protein cages remained intact and metallic cores were surrounded by a protein shell (Figure 2d). The presence of the apoferritin shell prevents irreversible aggregation of metallic nanoparticles and makes them water-soluble. It should be noted that the preparation of CoNi nanoparticles in apoferritin-free media resulted in bulk precipitation of a black solid. No electron diffraction pattern was obtained, suggesting an amorphous material. The X-ray diffractogram of powder samples confirmed an amorphous material (data not shown).

When studying bimetallic systems, the first question to ask is if the two metals are really combined in every nanoparticle. EDX measurements show the presence of Co and Ni but did not give information about how these metals were distributed inside each nanoparticle. To answer this question, we used EEL spectroscopy. We analyzed a series of nanoparticles using the so-called SL technique. Figure 3 illustrates the results obtained when a 0.5 nm probe is scanned across two individual nanoparticles of the $Co_{25}Ni_{75}$ sample (Figure 3a). The 3D illustration of the acquired spectra, in the 500−950 eV energy range, taken along the A−B line shows the Co−$L_{2,3}$ and Ni−$L_{2,3}$ edges signal (780 and 853 eV, respectively) variation as we go across the two nanoparticles. Note how Co and Ni metals are associated in both nanoparticles and the O−K signal is not observed in the spectra (Figure3b). The intensity line profile (Figure 3c) shows the HAADF variation along the particles, a signal that can be related to the projected sample mass. EELS spectra were quantified using standard methods,[19] and the Co (red line) and Ni (black line) chemical composition along both particles was determined (Figure 3d). EELS results clearly showed the presence of both metals, which are intimately associated in these nanoparticles.

Magnetic properties were characterized by SQUID measurements (Figure 4). ZFC/FC magnetization curves were performed as a function of the temperature (2−300 K) at a field of H = 50 Oe (Figure 4a). We observed maxima in the ZFC curves for all CoNi samples. The obtained blocking temperatures (T_B) vary from 11 to 70 K, as the Co content increases, and delimit the ferromagnetic−superparamagnetic transition. Above the blocking temperature, the ZFC and FC curves superimpose perfectly, so we can rule out the presence of much aggregation in all of these samples. It is worthy to note that CoNi−apoferritin T_B values range between 6 and 70, which are the T_B values previously reported for pure Ni− and Co−apoferritin nanoparticles, respectively.[20] The presence of only one clearly defined peak in the ZFC curve is a further argument in favor of the formation of bimetallic CoNi NPs, with almost homogeneous chemical and physical properties.[21]

(19) Egerton, R. F. *Electron Energy-Loss Spectroscopy in the Electron Microscope*, 2nd ed.; Plenum Press: New York, 1996.
(20) Gálvez, N.; Sánchez, P.; Domínguez-Vera, J. M.; Soriano-Portillo, A.; Clemente-León, M.; Coronado, E. *J. Mater. Chem.* **2006**, *16*, 2757.
(21) Poddar, P.; Srinath, S.; Gass, J.; Prasad, B. L. V.; Srikanth, H. *J. Phys. Chem. C* **2007**, *111*, 14060.

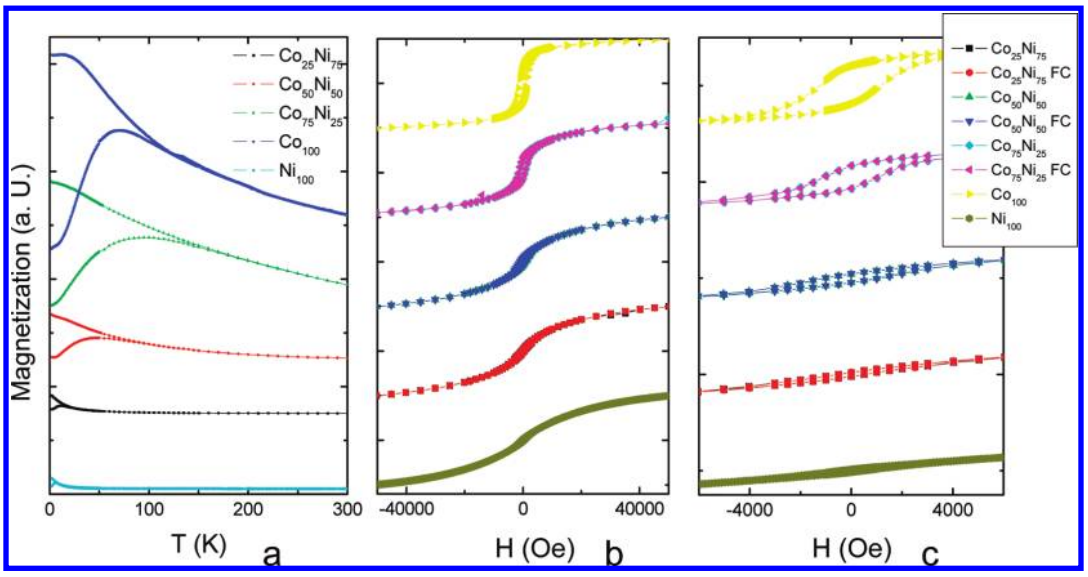

Figure 4. (a) Field-cooled (FC) and zero-field-cooled (ZFC) curves for CoNi samples at 50 Oe. (b) Hysteresis loops recorded at 2 K and hysteresis loops recorded at 2 K in a field cooled at 5 T. (c) Zoom of the M−H curves showing H_C and the absences of exchange-bias shift.

Table 2. Magnetic Properties: Remanence Magnetization (M_R/M_S), Coercive Field (H_C) and Blocking Temperature (T_B) of the CoNi Series[a]

	M_R/M_S (2 K)	H_C (Oe)	T_B (K)	initial Co/Ni	final Co/Ni
$Co_{25}Ni_{75}$	0.0364	500	11	0.33	0.46
$Co_{50}Ni_{50}$	0.07826	1000	40	1	0.95
$Co_{75}Ni_{25}$	0.21905	1100	80	3	3.3
[b]Co_{100}	0.39888	1250	70		
[b]Ni_{100}	0.0264	390	6	0	0

[a] Initial Co/Ni molar ratio introduced during the synthesis and final Co/Ni atomic ratio obtained by atomic absorption spectroscopy. [b] Previously reported data, ref 20.

Figure 4b shows the hysteresis loops recorded at 2 K, that is, below the blocking temperature. The CoNi particles show ferromagnetic behavior at this temperature. The magnetization curves measured versus applied fields reflect the particle anisotropy. A remanence of the saturation ($M_R/M_S < 0.5$) is found for all of the samples (Table 2). This value is characteristic of an assembly of randomly oriented single-domain uniaxial particles. The coercivity increases in the range between 500 and 1100 Oe when the cobalt content increases. In any case, H_C values range between the 390 Oe for pure Ni nanoparticles and 1200 Oe for pure Co nanoparticles.[20] Hysteresis curves recorded in the field-cooled regime (5 T) did not show a shift of the loops, evidencing the lack of exchange bias coupling (H_{EB}). Magnetization recorded at 300 K did not show coercive fields or remanence magnetization, characteristics of a superparamagnetic behavior (data not shown). In Table 2 are summarized the main magnetic properties of CoNi−apoferritin nanoparticles compared with pure Ni and Co−apoferritin phases. H_C and T_B values are in good agreement with previous published data for similar CoNi compositions and sizes.[6,7]

An interesting issue in the CoNi system upon oxidation is the possibility of forming core−shell structures (Co/CoO, Ni/NiO, Co/NiO, or Ni/CoO) exhibiting exchange bias coupling, an effect in which the antiferromagnetic shells (CoO or NiO) enhance the effective magnetic anisotropy of the cores (Co or Ni). So, we performed a structural and magnetic characterization of the same CoNi samples after intentional oxidation in an air atmosphere.

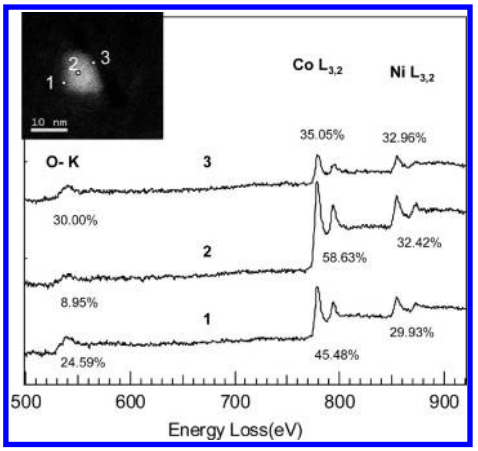

Figure 5. EEL spectra at the energy loss region of O−K, Co−$L_{2,3}$, and Ni−$L_{2,3}$ edges, extracted from the spectrum line acquired at the $Co_{75}Ni_{25}$ sample (inset: STEM-HAADF image).

Figure 5 shows the results extracted from a SL-EELS analysis, 50 spectra with an energy dispersion of 0.5 eV and an acquisition time of 2 s per spectrum were acquired when a 0.5 nm probe was scanned across individual nanoparticles (see inset figure). O−K, Co−$L_{2,3}$, and Ni−$L_{2,3}$ signals are present all along the nanoparticle. Note how in spectra 1 and 3 (Figure 5), which correspond to surface locations, the O peak is more intense than in spectra 2, corresponding to the nanoparticle core, meaning that oxygen is located, mainly, at the surface. The O, Co, and Ni quantification was carried out analyzing the O−K, Co−$L_{2,3}$, and Ni−$L_{2,3}$ signals. A power law model for the background subtraction and a Hartree−Slater model for the cross-section were applied.[19]

We focused on the change observed in EELS after the oxidation process. Briefly, the results suggested that we had oxidation of CoNi nanoparticles, at least partially, and that the oxidation was mainly localized at the surface of the nanoparticles. Therefore, we used the high sensitivity of the X-ray near-edge structure (XANES) spectroscopic technique

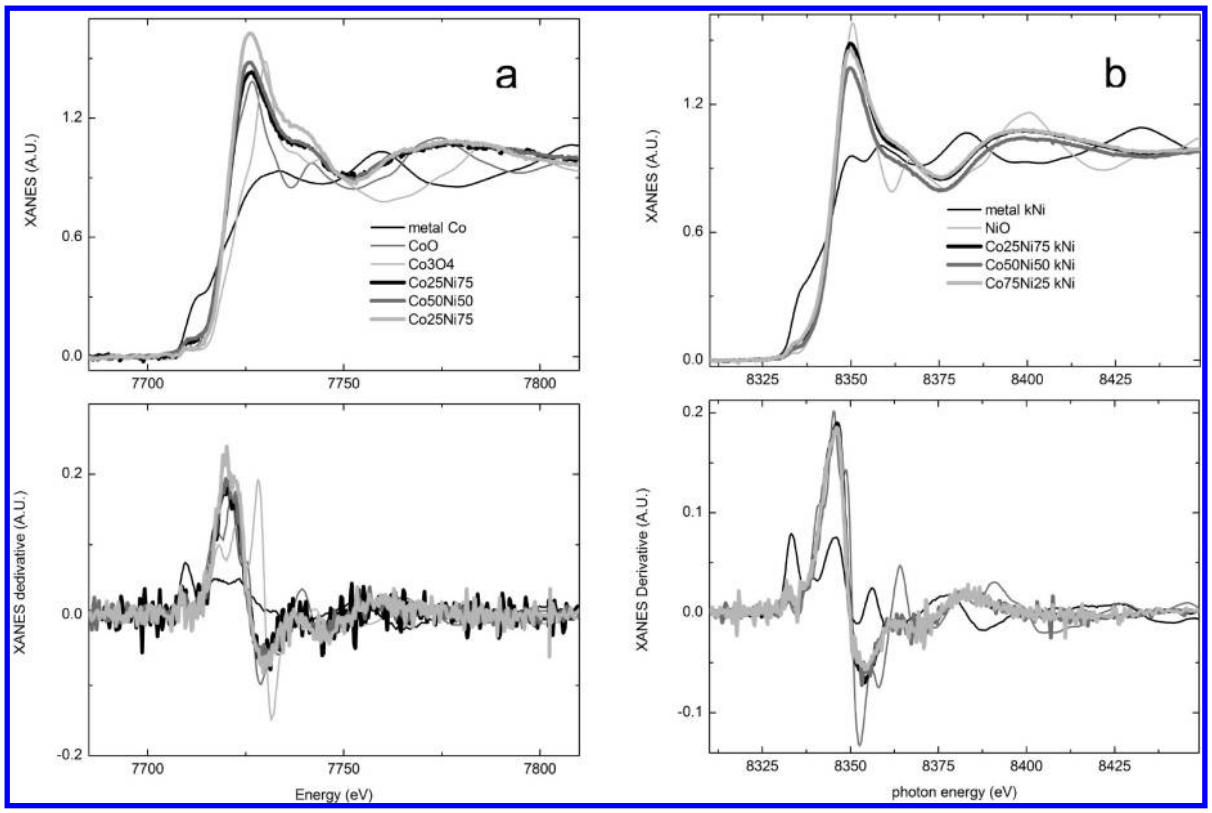

Figure 6. XANES spectra (upper panel) and their first derivatives (lower panel) of the CoNi series at the Co−K edge (a) and at the Ni−K edge (b).

Table 3. Proportion of Co, Co_3O_4, $Co(OH)_2$, Ni, and NiO in the CoNi Series Extracted from XANES Experiments

	% $Co(OH)_2$	% Co	% Co_3O_4	% Ni	% NiO
$Co_{25}Ni_{75}$	38 ± 1	13 ± 1	49 ± 1	23 ± 1	77 ± 1
$Co_{50}Ni_{50}$	41 ± 1	10 ± 1	49 ± 1	23 ± 1	77 ± 1
$Co_{75}Ni_{25}$	37 ± 1	26 ± 1	37 ± 1	28 ± 2	72 ± 2

to gain information about the oxidation state and chemical nature of the CoNi−apoferritin species. XANES results are shown in Figure 6a, cobalt K-edge, and 6b, nickel K-edge, together with the corresponding reference spectra, Co, Co_3O_4, $Co(OH)_2$, Ni, and NiO, for comparison. Solid thick lines correspond to the spectra obtained for the CoNi samples, and solid thin lines correspond to the reference spectra (Figure S1, in the Supporting Information, show the corresponding EXAFS spectra). Both the overall shape and structure of the spectra and their derivatives clearly indicate that the CoNi species consist of a mixture of oxides and metallic nanoparticles. Detailed least-squares fits of the XANES data (not shown) indicate that Co is present as Co, Co_3O_4, and $Co(OH)_2$ and Ni as Ni and NiO, being the oxides the main phases (Table 3).

The blocking temperature (T_B; Figure 7a) for oxidized samples varies from <2 to 60 K as the Co content increases. The lower T_B values of oxidized samples with respect to pure bimetallic ones are in agreement with oxide formation.[21,7]

The hysteresis curves (Figure 7b) show coercivity values for oxidized samples varying between 80 and 500 Oe when the cobalt content increases. In Table 4 are collected the H_C, T_B, and M_R values for oxidized samples. The lower values obtained for H_C, as well as the slightly higher values obtained for M_S (saturation magnetization), as compared with nonoxidized samples, are coherent with an oxidation of the metal phase. The higher M_S values are, probably, due to an increase of paramagnetic species.[22,23] Magnetization curves recorded in the field cooled regime (5 T) did not show exchange bias coupling (Figure 7c). The exchange bias coupling occurs in core−shell structures when a ferromagnet (FM core) shares an interface with an antiferromanget (AFM shell) having a larger magnetic anisotropy, and the AFM pins the orientation of the moment in the FM layer (through exchange interaction), which results in an enhanced coercivity and an asymmetric shift of the hysteresis loop (H_{EB}). This effect depends on the quality of the FM/AFM interface coupling, which is closely related to the crystallinity of the core−shell and the nanoparticle shape. In our samples, despite the presence of Ni and Co oxides, observed by XANES, and that EELS suggested an increase of oxygen in particle surface locations, no evidence of an exchange bias shift was found. Probably, no proper core−shell structure formation and poor crystallinity are responsible for a weak FM/AFM interface coupling. The amorphous structure combined with a lack of thickness renders the AFM shells unable to support the interfacial pinning strength necessary for an exchange shift.[25,26] Finally, the fact that Co_3O_4 oxide is

(22) Verelst, M.; Ould Ely, T.; Amiens, C.; Snoeck, E.; Lecante, P.; Mosset, A.; Respaud, M.; Broto, J. M.; Chaudret, B. *Chem. Mater.* **1999**, *11*, 2702.
(23) Chen, J. P.; Sorensen, C. M.; Klabunde, K. J.; Hadjipanayis, G. C. *Phys. Rev. B* **1995**, *51*, 11527.
(24) Zhou, Y. Z.; Chen, J. S.; Tay, B. K.; Hu, J. F.; Chow, G. M.; Liu, T.; Yang, P. *Appl. Phys. Lett.* **2007**, *90*, 043111.
(25) Nogués, J.; Skumryev, V.; Sort, J.; Stoyanov, S.; Givord, D. *Phys. Rev. Lett.* **2006**, *97*, 157203.
(26) Tracy, J. B.; Weiss, D. N.; Dinega, D. P.; Bavwendi, M. G. *Phys. Rev. B* **2005**, *72*, 064404.

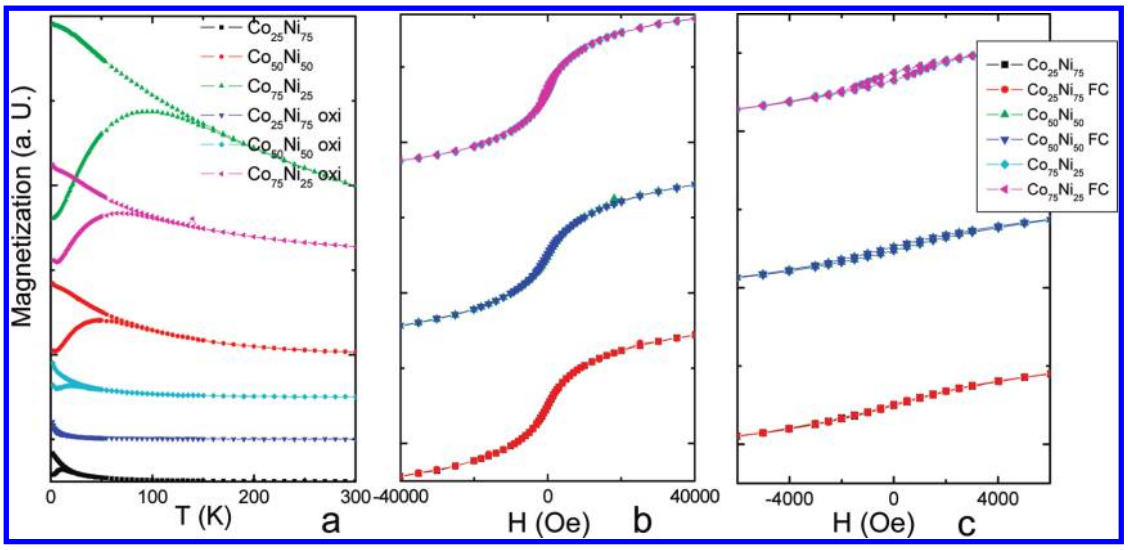

Figure 7. (a) Field-cooled (FC) and zero-field-cooled (ZFC) curves for oxidized CoNi samples at 50 Oe. (b) Hysteresis loops recorded at 2 K and hysteresis loops recorded at 2 K in a field cooled at 5 T. (c) Zoom of the M−H curves showing H_C and the absences of exchange-bias shift.

Table 4. Magnetic Properties: Remanence Magnetization (M_R/M_S), Coercive Field (H_C), and Blocking Temperature (T_B) of Oxidized Samples

oxidized	M_R/M_S (2 K)	H_C (Oe)	T_B (K)
$Co_{25}Ni_{75}$	0.00848	80	No
$Co_{50}Ni_{50}$	0.022	270	20
$Co_{75}Ni_{25}$	0.05	500	90

less effective than CoO oxide in producing exchange bias coupling[27] could be claimed as another contributing factor, keeping in mind that the factors determining the strength of the exchange bias interaction remain incomplete.

Conclusions

In this work, the preparation of CoNi nanoparticles of different compositions encapsulated within the apoferritin cavity have been reported. We have shown the convenience of using apoferritin protein as a confined medium where bimetallic nanoparticles can be synthesized under mild chemical conditions. Only a few examples in the literature can be found related to the chemical preparation of bimetallic CoNi nanoparticles, highlighting the importance of finding new synthetic routes. In this sense, biomimetic methods that occur in water are easier and "friendlier" than nonhydrolytic synthetic methods and therefore offer an interesting approach to metallic nanoparticle synthesis. The three CoNi series showed important H_C and T_B values, varying with composition. These are crucial magnetic properties if one thinks in terms of biomedical applications. Upon oxidation, the CoNi series have decreased superparmagnetic blocking temperatures (T_B) and coercivity (H_C), and no exchange bias shift (H_{EB}) is observed. Probably, a lack of proper core−shell structure formation, poor crystallinity, and the presence of Co_3O_4 instead of CoO oxide are the factors responsible for a weak FM/AFM interface coupling. But still, coercive and T_B values remain of significant importance proving the use of apoferritin protein as a good template for the synthesis of metallic or oxide nanoparticles.

Acknowledgment. We are grateful to the MEC (project CTQ2006-02840), Junta de Andalucía (Proyecto Excelencia FQM-02525), and EU I3 Project ESTEEM (contract no. 026019 RII3) for financial support. N.G. and S.T. thank the MEC for a research contract (Ramón y Cajal program).

Supporting Information Available: (Figure S1) k2-weighted EXAFS spectra (panel A, nickel K-edge; panel B, cobalt K-edge) and Fourier transform of the spectra in panels A and B (panel C, nickel K-edge; panel D, cobalt K-edge). This material is available free of charge via the Internet at http://pubs.acs.org.

(27) Srikala, D.; Singh, V. N.; Banerjee, A.; Mehta, B. R.; Patnaik, S. *J. Phys. Chem. C* **2008**, *112*, 13882.